

dc-electric-field-induced and low-frequency electromodulation second-harmonic generation spectroscopy of Si(001)-SiO₂ interfaces

O. A. Aktsipetrov,* A. A. Fedyanin, A. V. Melnikov, E. D. Mishina, and A. N. Rubtsov
Department of Physics, Moscow State University, Moscow 119899, Russia

M. H. Anderson, P. T. Wilson, M. ter Beek, X. F. Hu, J. I. Dadap,[†] and M. C. Downer
Department of Physics, The University of Texas at Austin, Austin, TX 78712

(Received 7 May 1998; revised manuscript received 5 January 1999)

The mechanism of dc-electric-field-induced second-harmonic (EFISH) generation at weakly nonlinear buried Si(001)-SiO₂ interfaces is studied experimentally in planar Si(001)-SiO₂-Cr MOS structures by optical second-harmonic generation spectroscopy with a tunable Ti:sapphire femtosecond laser. The spectral dependence of the EFISH contribution near the direct two-photon E_1 transition of silicon is extracted. A systematic phenomenological model of the EFISH phenomenon, including a detailed description of the space-charge region (SCR) at the semiconductor-dielectric interface in accumulation, depletion, and inversion regimes, has been developed. The influence of surface quantization effects, interface states, charge traps in the oxide layer, doping concentration, and oxide thickness on nonlocal screening of the dc-electric field and on breaking of inversion symmetry in the SCR is considered. The model describes EFISH generation in the SCR using a Green's-function formalism which takes into account all retardation and absorption effects of the fundamental and second-harmonic (SH) waves, and multiple reflection interference in the SiO₂ layer. The optical interference between field-dependent and -independent contributions to the SH field is considered as an *internal homodyne* amplifier of the EFISH effects. Good agreement between the phenomenological model and our EFISH spectroscopic results is demonstrated. Finally, low-frequency electromodulated EFISH is demonstrated as a useful differential spectroscopic technique for studies of the Si-SiO₂ interface in silicon-based metal-oxide-semiconductor structures. [S0163-1829(99)01836-6]

I. INTRODUCTION

Optical second harmonic generation (SHG) has been one of the most intensively studied phenomena in surface and interface optics¹⁻³ for the last decade. The interest in SHG stems from its unique sensitivity to the structural and electronic properties of surfaces and interfaces of centrosymmetric media. This unusually high surface/interface sensitivity comes about because, in the electric dipole approximation, SHG is forbidden in the bulk of materials with inversion symmetry,^{4,5} but allowed at interfaces, where inversion symmetry is broken by the discontinuity of crystalline structure. Related nonlinear sources of SHG are localized in a thin (several nanometers thick) surface or interface layer. In semiconductors, inversion symmetry is also broken by the dc electric field (DCF) in the subsurface space-charge region (SCR), which is created by initial band bending and/or external bias application. The lack of inversion symmetry in the SCR results in dc-electric-field-induced second-harmonic (EFISH) generation, which manifests itself through electro-modulation of the SHG intensity. Thus, all important properties of surfaces, buried interfaces and subsurface layers—their charge,⁶⁻⁸ electronic surface state density,⁹⁻¹² roughness (morphology),^{13,14} adsorption (adatom and admolecule surface density),¹⁵⁻¹⁸ initial band bending,¹⁹⁻²¹ etc.—can, in principle, be determined by means of the SHG probe.

The technological importance of Si(001)-SiO₂ interfaces stems from their ubiquitous presence in metal-oxide-semiconductor (MOS) structures and MOS field-effect transistors. EFISH generation provides a promising noninvasive,

in situ technique for characterizing interfacial imperfections and charge defects at the Si(001)-SiO₂ interface. Moreover, the relative simplicity of the description of the SHG response from the Si(001) face, originating from the small number of tensor components of the interface quadratic susceptibility and the rotationally isotropic interfacial SHG response, makes the Si(001)-SiO₂ interface among the most important for investigation of fundamental aspects of the EFISH phenomenon.

The 1967 discovery of EFISH generation by Lee *et al.*²² at Si- and Ag-electrolyte interfaces in electrochemical cells remained largely unnoticed for a number of years. The 1981 discovery of surface-enhanced SHG by Shen *et al.*²³ rejuvenated interest in this effect. Surface-enhanced EFISH generation at a silver-electrolyte interface was observed shortly afterward.²⁴ Since 1984, EFISH has been systematically studied at Si(111)-electrolyte interfaces,²⁵⁻²⁹ and to a lesser extent at other semiconductor-electrolyte interfaces: Cd₃P₂(111),³⁰ CdIn₂S₄(111),³¹ GaN(001),³² and TiO₂.³³ These studies revealed that the strength of the dc electric field which could be applied electrochemically was limited by interface electrochemical reactions, such as oxidation of a silicon surface at anodic potential. To circumvent this restriction, EFISH generation studies were extended to Si-SiO₂ MOS structures with bias applied by a ring metal³⁴ or a semitransparent Cr (Refs. 20 and 35) gate electrode, and to GaAs-based MOS structures.³⁶ This technique of the dc-electric-field application in nonlinear-optical experiments was extended recently to the studies of the dc-electric-field-induced fourth- and third-harmonic generation,³⁷ and al-

lowed the development of an interesting SHG interferometry: frequency-domain interferometric EFISH spectroscopy.³⁸

A simple phenomenological model of EFISH based on the ‘‘interface field approximation’’—which assumes a linear dependence of the dc-field-induced nonlinear polarization on interface DCF strength, and yields a quadratic dependence of EFISH intensity on bias voltage—was developed for the Si-SiO₂-electrolyte interface in Refs. 26 and 27. Since clear deviations from a quadratic bias dependence were observed,^{34,35} this model was improved by taking into account the nonlinear interference of dc-field-induced and field-independent contributions to the nonlinear quadratic polarization as well as retardation and absorption effects.³⁵ Further improvement resulted from considering the spatial inhomogeneity of the DCF and the dc-electric-field-induced contribution to the nonlinear polarization.³⁵ These effects were later analyzed with a Green-function formalism.^{39,40} At present, the most comprehensive description of the EFISH phenomenon was presented in Ref. 40. However, this analysis remains incomplete on three points. First, it is restricted to the depletion regime of the SCR, whereas experimentally applied biases have included accumulation and inversion regimes. Moreover, as we demonstrate in this paper, the transition from depletion to inversion to accumulation drastically changes the EFISH response. Second, surface quantization effects originating from strong-field localization in inversion and accumulation regimes, as well as the role of interface states, should be taken into account. Third, multiple reflection interference in the SiO₂ layer, which significantly affects the SHG intensity from Si-SiO₂ structures,^{41–43} was neglected.

In this paper we present a comprehensive phenomenological model of EFISH generation supported by experimental spectroscopic studies of *p*- and *n*-type Si(001)-SiO₂-Cr MOS structures. The key features of our model are (1) a detailed electrophysical model of the SCR in the accumulation and inversion regimes, which takes into account interface states and oxide charge traps and their effect on the spatial DCF distribution in the SCR; (2) a rigorous nonlinear optical model of EFISH in the SCR, based on a Green’s-function formalism, which takes into account all retardation effects, absorption of the fundamental and SH radiation, multiple reflection interference of both the fundamental and SH waves in the oxide and optical interference between field- and field-independent contributions to the SH field. The latter interference effect, considered here as an internal homodyne amplifier of the EFISH contribution to the total SHG response, was considered in Refs. 44 and 45 for an external reference. The key feature of our experiments is comprehensive observation of the dependence of SHG on numerous parameters, including applied bias, azimuthal sample rotation, wavelength near the direct two-photon E_1 transition, doping concentration, and oxide thickness. These combined dependences allow us to deconvolve the EFISH contribution fully from field-independent contributions. The nonquadratic bias dependence of the EFISH intensity predicted in Refs. 33 and 40, and its variation with doping concentration, oxide thickness, interfacial state density, and wavelength, is observed and analyzed in detail.

II. THEORETICAL BACKGROUND

A. Quadratic optical response of the Si-SiO₂ system

In the presence of a DCF the nonlinear polarization $\mathbf{P}(\mathbf{r}, t)$ of a centrosymmetric semi-infinite semiconductor at the second-harmonic (SH) frequency 2ω is given by^{46,47}

$$\mathbf{P}^{NL}(\mathbf{r}, 2\omega) = \mathbf{P}^S(\mathbf{r}, 2\omega) + \mathbf{P}^{BQ}(\mathbf{r}, 2\omega) + \mathbf{P}^{BD}(\mathbf{r}, 2\omega), \quad (1)$$

where ω is the frequency of the fundamental radiation, \mathbf{r} is the radius vector of a nonlinear source location inside the semiconductor, $\mathbf{P}^S(\mathbf{r}, 2\omega)$ is the surface nonlinear polarization, $\mathbf{P}^{BQ}(\mathbf{r}, 2\omega)$ is the bulk quadrupole contribution, and $\mathbf{P}^{BD}(\mathbf{r}, 2\omega)$ is the bulk dipole DCF-induced polarization. The last contribution is governed by the fourth-rank cubic susceptibility tensor $\chi^{(3)}$, and can be written phenomenologically as

$$\mathbf{P}^{BD}(\mathbf{r}, 2\omega) = \chi^{(3),BD}(2\omega; \omega, \omega, 0) : \mathbf{E}(\mathbf{r}, \omega) \mathbf{E}(\mathbf{r}, \omega) \mathbf{E}_0(\mathbf{r}), \quad (2)$$

where $\mathbf{E}(\mathbf{r}, \omega)$ is the amplitude of the fundamental optical field inside the semiconductor, which is \mathbf{r} dependent due to optical absorption, and $\mathbf{E}_0(\mathbf{r})$ is the amplitude of the dc electric field in the semiconductor SCR which is \mathbf{r} dependent due to screening of the dc electric field by free carriers. In Eq. (2) we consider the local relationship between $\mathbf{P}^{BD}(\mathbf{r}, 2\omega)$ and $\mathbf{E}(\mathbf{r}, \omega)$ and $\mathbf{E}_0(\mathbf{r})$. This approximation is valid for the bulk of the semiconductor, where nonlocality related to the spatial dispersion for the fundamental field is small and the screening length of the dc electric field is much larger than a lattice parameter. For strong accumulation and strong inversion regimes, as the screening length is of the order of a lattice parameter, we consider nonlocal screening of the DCF which takes into account quantum size effects in a subsurface quantum well (Sec. II D).

The bulk quadrupole contribution in the plane-wave approximation is given by

$$\mathbf{P}^{BQ}(\mathbf{r}, 2\omega) = \chi^{(2),BQ}(2\omega; \omega, \omega) : \mathbf{E}(\mathbf{r}, \omega) i \mathbf{k}_\omega \mathbf{E}(\mathbf{r}, \omega), \quad (3)$$

where $\chi^{(2),BQ}$ is a fourth-rank tensor which represents the quadrupole contribution to the quadratic nonlinear susceptibility from spatial dispersion, and \mathbf{k}_ω is the wave vector of the fundamental radiation in the semiconductor. $\chi^{(2),BQ}$ has the same symmetry properties as $\chi^{(3),BD}$.

For the surface contribution to \mathbf{P}^{NL} the multipole expansion is hardly expected to be valid, and we suppose that⁴⁸

$$\begin{aligned} \mathbf{P}^S(\mathbf{r}, 2\omega) &= \chi_{eff}^{(2),S}(2\omega; \omega, \omega) : \mathbf{E}(\omega, z=0_+) \mathbf{E}(\omega, z=0_+) \\ &= \delta(0_+) \int_0^{z_{surf}} \chi^{(2),S}(z') \mathbf{E}(z', \omega) \mathbf{E}(z', \omega) dz', \end{aligned} \quad (4)$$

where $\chi_{eff}^{(2),S}$, a third-rank tensor, is an effective quadratic susceptibility of the surface layer resulting from the integration of the right-hand side of Eq. (4), which includes an inhomogeneous susceptibility $\chi^{(2),S}(z')$ of a subsurface layer with thickness z_{surf} , and $z=0_+$ denotes a position near the interface just inside the semiconductor. The integral in Eq. (4) consists of a local part from the breaking of the inversion symmetry at the surface, and a nonlocal part from

the discontinuity of the normal electric-field component at the surface. The thickness z_{surf} of the subsurface layer, from which $\mathbf{P}^S(\mathbf{r}, 2\omega)$ originates, is determined by the region where either electron motion remains sensitive to the breakdown of inversion symmetry or where the normal electric-field component changes from its vacuum (oxide) magnitude to that in the silicon bulk. An estimation of z_{surf} is approximately 2–3 atomic layers, based on the experiments by Heinz *et al.*¹⁵ on SHG from reconstructed Si surfaces. They showed that the surface contribution to the SHG response arises almost entirely from the reconstructed surface layer with a thickness that, as proven by scanning tunneling microscopy, does not exceed 2–3 topmost atomic layers. The structure of $\chi^{(2),S}$ and $\chi^{(2)}(z)$ depends on the particular crystalline face under consideration. Hereafter we use the \mathbf{xyz} coordinate frame, with the \mathbf{xy} plane coinciding with the interface and the positive \mathbf{z} axis directed toward the semiconductor bulk.

The SH electromagnetic field $\mathbf{E}(\mathbf{R}, t) = \mathbf{E}(\mathbf{R}, 2\omega) \exp i(2\omega t - \mathbf{k}_{2\omega} \mathbf{R})$, where $\mathbf{E}(\mathbf{R}, 2\omega)$ is the amplitude of the SH field at the point of observation \mathbf{R} , can be found by solving the inhomogeneous wave equation for propagation of the SH wave with \mathbf{P}^{NL} as a source term.^{48,49} The solution can be written formally in terms of the tensorial Green function $\vec{G}(\mathbf{R}, \mathbf{r}', 2\omega)$, which is defined to be the solution of the wave equation with a point source at \mathbf{r}' . Expressions for the components of \vec{G} , are calculated in Refs. 43 and 44. The SH field $\mathbf{E}(2\omega)$ in the point of detection \mathbf{R} is given by

$$\mathbf{E}(\mathbf{R}, 2\omega) = \int \vec{G}(\mathbf{R}, \mathbf{r}', 2\omega) \mathbf{P}^{NL}(\mathbf{r}', 2\omega) d\mathbf{r}', \quad (5)$$

where integration is taken over the bulk of the semiconductor. Since translational symmetry in the interface plane is assumed, the DCF-induced part of the SH field is given by

$$\begin{aligned} \mathbf{E}^{BD}(\mathbf{R}, 2\omega) &= F_{2\omega} F_{\omega}^2 \chi_{eff}^{BD} I_{\omega} \mathbf{p} \exp(i\mathbf{k}_{2\omega} \mathbf{R}) \\ &\times \int_0^{+\infty} E_0(z') \exp[i(k_{2\omega, z} + 2k_{\omega, z})z'] dz', \end{aligned} \quad (6)$$

where $\mathbf{k}_{2\omega}$ is the SH wave vector, the scalar factor χ_{eff}^{BD} is a linear combination of components of $\chi^{(3),BD}$ which depends on the experimental geometry,²¹ I_{ω} is the intensity of the fundamental radiation, and $k_{\omega, z}$ and $k_{2\omega, z}$ are the normal wave-vector components of the fundamental and SHG radiation, respectively, in the semiconductor. The unit vector \mathbf{p} defines the polarization of the EFISH field, and F_{ω} and $F_{2\omega}$ are the transmission factors which include Fresnel coefficients and a correction for multiple reflections in the silicon oxide at both ω and 2ω . Equation (6) properly takes into account retardation, the penetration depth of the fundamental wave, the escape length of the SH wave, and multiple reflection interference effects in oxide layer.

B. dc-electric-field spatial distribution

To perform the integration in Eq. (6) one must know the spatial distribution $E_0(z)$ across the SCR. In this section we

consider the screening of this DCF within the framework of Fermi carrier statistics.^{50–52} The spatial distribution of the electrostatic potential $\varphi(z)$ in the planar semiconductor-dielectric system can be found as a solution of the one-dimensional Poisson equation

$$\frac{\partial}{\partial z} \left(\epsilon \frac{\partial \varphi}{\partial z} \right) = -4\pi n, \quad (7)$$

where $\epsilon = \epsilon_{sc}(\epsilon_d)$ is the static dielectric constant of the semiconductor (dielectric) and $n = n(z)$ is the space-charge density. The boundary conditions for Eq. (7) are

$$\begin{aligned} \varphi(+\infty) &= \mu, \\ \varphi(-D) &= \mu + U, \end{aligned} \quad (8)$$

where μ is the chemical potential of the semiconductor and D is the thickness of the oxide film. The first of Eq. (8) is a statement of charge neutrality in the bulk of the semiconductor. The second equation takes into account the application of external bias voltage U to the metal electrode with respect to the semiconductor. We divide the charge density into field-independent and -dependent terms

$$n = n_{fi} + n_{fd}, \quad (9)$$

where n_{fi} includes the density of the ionized donors N_D and acceptors N_A , and a fixed charge n_{ox} trapped in the oxide layer near the semiconductor-dielectric interface:

$$n_{fi} = N_D + N_A + \delta(0_-) n_{ox}, \quad z \geq 0, \quad (10)$$

where $z=0_-$ is a position near the interface just inside the dielectric.

The spatial distribution $n_{fd}(z)$ is, in principle, a nonlinear functional of the potential φ at all points inside the semiconductor. However, if the potential dependence on the coordinate is slow enough, which is true for all except very high biases, the screening can be treated locally. In this way we find expressions for $n_{fd}(z)$ and $E_0(z)$ within the model of local screening of the DCF in a Fermi electron-hole gas, in which $n_{fd}(z)$ depends on the potential φ at point z , i.e., $n_{fd}(\varphi) = n_{fd}[\varphi(z)]$. The case of nonlocal screening is considered in Sec. II C. The field-dependent part of the charge density consists of the density of holes, n_h , the density of electrons, n_e , and interface traps n_{it} , which depend on the interface potential:

$$\begin{aligned} n_{fd}(z) &= n_h[\varphi(z)] + n_e[\varphi(z)] \\ &+ \delta(0_+) n_{it}[\varphi(z=0_+)], \quad z \geq 0. \end{aligned} \quad (11)$$

Since we assume that the SHG response comes from the semiconductor or semiconductor-dielectric interface, we treat charges in the oxide layer as an effective fixed trapped charge n_{ox} . Since at $z > 0$ the variable z does not enter into Eqs. (10) and (11) explicitly, and the charge density n_{fd} depends on the coordinate via $\varphi(z)$, the Poisson equation (7) has the first integral

$$E_0^2(\varphi) = \frac{8\pi}{\epsilon} \int_{\varphi}^{\mu} n(\varphi') d\varphi'. \quad (12)$$

Using the charge neutrality condition in the bulk of the semiconductor for completely ionized donors and acceptors yields

$$N_D + N_A = n_0 + p_0, \quad (13)$$

where n_0 and p_0 are the densities of electrons and holes in conduction and valence bands, respectively, in the absence of the external field. Then

$$N_D + N_A = eN_C \Phi\left(\frac{\mu - \varepsilon_C}{kT}\right) - eN_V \Phi\left(\frac{\varepsilon_V - \mu}{kT}\right), \quad (14)$$

where N_V and N_C are the effective densities of states in valence and conduction bands, respectively, ε_V and ε_C are the energies of the upper level of the valence band and the lower level of the conduction band, respectively, k is the Boltzmann constant, and T is the temperature. Effective densities of states $N_V = 2(2\pi m_h kT)^{3/2}$ and $N_C = 2M_C(2\pi m_e kT)^{3/2}$, where M_C is the number of equivalent minima in the conduction band, depend on the effective mass of electrons m_e or holes m_h , and temperature.⁵³ For silicon $M_C = 6$, and following Sze,⁵² we take $N_V = 1.04 \times 10^{19} \text{ cm}^{-3}$ and $N_C = 2.8 \times 10^{19} \text{ cm}^{-3}$. $\Phi(\tau)$ is the Fermi-Dirac integral

$$\Phi(\tau) = \frac{2}{\sqrt{\pi}} \int_0^\infty \sqrt{x} [1 + \exp(x - \tau)]^{-1} dx. \quad (15)$$

Equations (10) and (11) have the form

$$n_{fd}[\varphi(z)] = eN_V \Phi\left(\frac{\varepsilon_V - \varphi}{kT}\right) - eN_C \Phi\left(\frac{\varphi - \varepsilon_C}{kT}\right) + \delta(0_+) n_{it}, \quad (16)$$

$$n_{fi} = eN_C \Phi\left(\frac{\mu - \varepsilon_C}{kT}\right) - eN_V \Phi\left(\frac{\varepsilon_V - \mu}{kT}\right) + \delta(0_-) n_{ox}. \quad (17)$$

Interface traps are charged midgap states at the semiconductor-dielectric interface resulting from interruption of the semiconductor lattice structure or interface imperfections. As the interface electrostatic potential changes, the trap levels move up or down while the Fermi level remains fixed. The interface trap density n_{it} is defined in terms of the energy distribution $L^{a,d}(\varepsilon)$ of trap levels across the semiconductor band gap and the density of traps per eV $N_{a,d}$:

$$n_{it}(\varphi) = e \int_{\varepsilon_V}^{\varepsilon_C} [N_d L^d(\varphi - \varepsilon) F^d(\varphi - \varepsilon) - N_a L^a(\varphi - \varepsilon) F^a(\varphi - \varepsilon)] d\varepsilon, \quad (18)$$

where superscripts a and d denote acceptor or donor traps, and

$$F^a(\tau) = \left[1 + \frac{1}{g^a} \exp\left(-\frac{\tau}{kT}\right) \right]^{-1}, \quad (19)$$

$$F^d(\tau) = \left[1 + g^d \exp\left(\frac{\tau}{kT}\right) \right]^{-1}. \quad (20)$$

Coefficients g^a and g^d reflect the ground-state degeneracy of the acceptor and donor levels. For silicon, due to the double degeneracy of valence bands in the center of Brillouin zone,⁵² we take $g^a = 4$ and $g^d = 2$. The specific form of $L^{a,d}(\varepsilon)$ depends on the preparation of the semiconductor-dielectric system. In the calculations we model this distribution as a set of Lorentz functions.

Spatial DCF and potential distributions can be found from the first integral $E_0(\varphi)$ [Eq. (12)] of the Poisson equation by integrating $z = \int_{\varphi}^{\varphi_{int} + \mu} [E_0(\varphi')]^{-1} d\varphi'$, with $\varphi_{int} = \varphi(z = 0_+) - \mu$. Figure 1 shows the distributions $\varphi(z)$ and $E_0(z)$ across the SCR of p -doped silicon. In the depletion regime, where the Schottky approximation is valid, $\varphi(z)$ is close to a parabolic function. For larger applied biases corresponding to inversion, the SCR divides into a thin subsurface region of rapidly changing potential, and a long tail of gradually decreasing potential. The transition depth z_0 between these two regions is several nanometers. In the accumulation regime, $\varphi(z)$ drops mostly within z_0 . Due to the large gradient of φ in this subsurface region, the relationship between φ and E_0 becomes nonlocal, and the first integral of the Poisson equation (12) is no longer valid. To find the DCF spatial distribution in this region, the self-consistent screening of the external dc electric field in subsurface quantum well should be considered.

C. Role of surface quantization effects in the subsurface region

The quantum effects in the screening of a DCF can be taken into account via self-consistent calculations,⁵⁴ using the Hartree-Fock (HF) approach to describe the electron exchange interaction. In the following we consider the screening of a ‘‘positive’’ (in the above notation) external potential in the subsurface region by electrons, with a negligible contribution from holes. The opposite case of a ‘‘negative’’ potential is treated similarly.

The HF equation for the single-electron wave function $\psi_i(\mathbf{r})$ is given by

$$\begin{aligned} \frac{\hat{p}^2}{2m} \psi_i(\mathbf{r}) + e^2 \sum_{j \neq i} \langle \psi_j(\mathbf{r}') | (\epsilon |\mathbf{r} - \mathbf{r}'|)^{-1} | \psi_j(\mathbf{r}') \rangle \psi_i(\mathbf{r}) \\ - e^2 \sum_{j \neq i, \parallel \text{spins}} \langle \psi_j(\mathbf{r}') | (\epsilon |\mathbf{r} - \mathbf{r}'|)^{-1} | \psi_i(\mathbf{r}') \rangle \psi_j(\mathbf{r}) \\ + V_0(\mathbf{r}) \psi_i(\mathbf{r}) = E_i \psi_i(\mathbf{r}), \end{aligned} \quad (21)$$

where $V_0(z) = -E_{0ext}z + \int n_{fi}(\mathbf{r}') (\epsilon |\mathbf{r} - \mathbf{r}'|)^{-1} d^3r'$, and the sum in the exchange (third) term is over states with parallel spins with brackets denoting an average over the stationary state; E_{0ext} is the strength of the (external) dc electric field inside the surface quantum well, and is a constant across the well.

Because of translation symmetry in the x, y plane, we put $\psi_i(\mathbf{r}) = \tilde{\varphi}_i(z) e^{i\mathbf{p}_i \cdot \mathbf{r}}$. We consider the case in which only one energy state \mathcal{E} for the subsurface electronic motion is responsible for most of the screening. The rest part of the screening occurs in the relatively thick layer, and can therefore be treated classically. This is confirmed by the numerical results. We also assume that $\tilde{\varphi}_i(z) \equiv \tilde{\varphi}(z)$ is independent of \mathbf{p}_i .

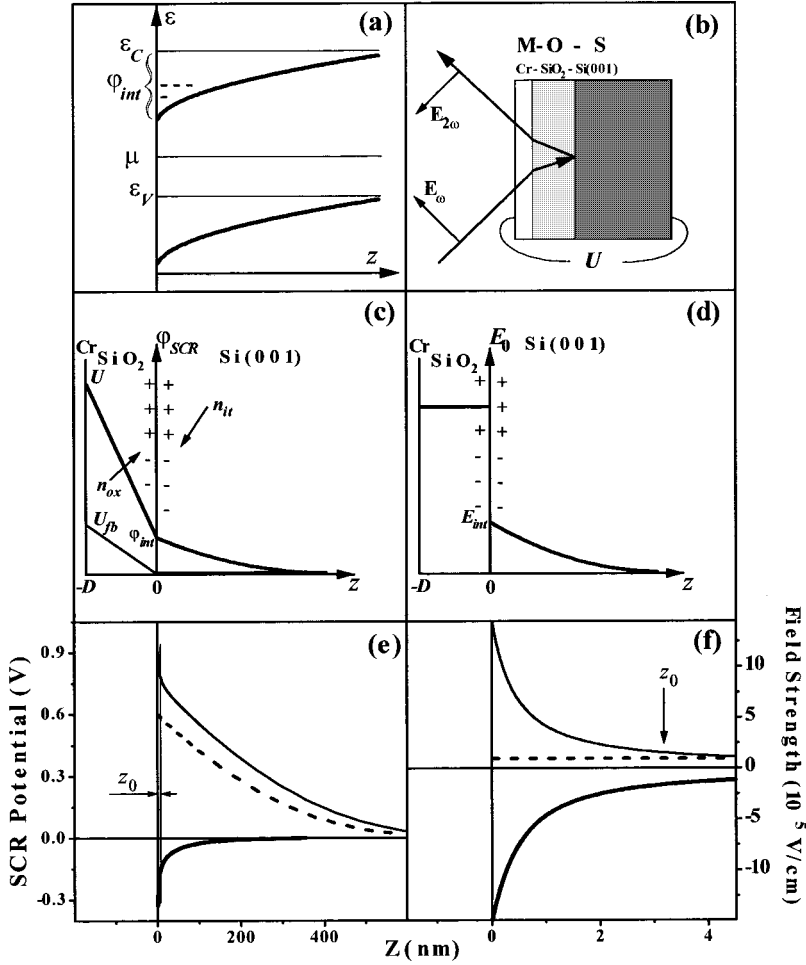


FIG. 1. Top panels: (a) The diagram of band bending near the surface of *p*-doped silicon for the depletion regime. The Fermi level μ , the energies of the upper level of the valence band ε_V , and the energies of the lower level of the conduction band ε_C in the silicon bulk are shown. (b) Schematic of the experimental geometry. Middle panels: sketches of the spatial distribution of the SCR potential $\varphi_{SCR}(z) = \varphi(z) - \mu$ [panel (c)] and DCF strength E_0 [panel (d)] across the MOS structure. Interface trap charges n_{it} and oxide charges n_{ox} are shown. The interface DCF E_{int} , interface potential φ_{int} , and applied bias U are depicted. The flatband voltage U_{fb} due to interface and oxide charges is shown. Bottom panels: (e) SCR potential and (f) DCF distributions across the SCR of *p*-doped silicon (doping concentration of $1.5 \times 10^{15} \text{ cm}^{-3}$) for three values of the interface potential: $\varphi_{int} = +0.95 \text{ V}$ (inversion) thin line, $\varphi_{int} = +0.6 \text{ V}$ (depletion) dashed line, and $\varphi_{int} = -0.33 \text{ V}$ (accumulation) thick line. The characteristic length z_0 of DCF screening in inversion and accumulation is marked.

Then Eq. (21) may be written in the form of a Schrödinger equation with self-consistent potential $U_{self}(z)$,

$$\mathcal{E}\tilde{\varphi}(z) = -\frac{\hbar^2}{2m} \frac{\partial^2}{\partial z^2} \tilde{\varphi}(z) - U_{self}(z) \tilde{\varphi}(z), \quad (22)$$

where

$$U_{self}(z) = -E_{0ext}z + \int \frac{n(\mathbf{r}')C(\mathbf{r}, \mathbf{r}') + n_{fi}(\mathbf{r}')}{\epsilon|\mathbf{r} - \mathbf{r}'|} d^3r', \quad (23)$$

$$n(\mathbf{r}) = \langle \hat{n}(\mathbf{r}) \rangle = e \sum_K \psi_K(\mathbf{r}) \psi_K^*(\mathbf{r}) f(E_K), \quad (24)$$

where $\hat{n}(\mathbf{r})$ is the density operator, $f(E_k) = 1/(1 + e^{(E_k - \mu)/kT})$ is the Fermi occupation factor, and

$$C(\mathbf{r} - \mathbf{r}') = 1 - \frac{e^2}{n(\mathbf{r})n(\mathbf{r}')} \times \sum_{j \neq i, ||spins} f(E_j) f(E_i) e^{i(\mathbf{p}_i - \mathbf{p}_j)(\mathbf{r} - \mathbf{r}')}. \quad (25)$$

$C(\mathbf{r} - \mathbf{r}')$ can be interpreted physically as a correlation function for the in-plane motion of electrons. Boundary conditions for the wave function are given by

$$\tilde{\varphi}(0) = 0, \quad \tilde{\varphi}(z_0) = 0. \quad (26)$$

Here we introduce the formal thickness z_0 of the subsurface region. At $z > z_0$ the screening is to be treated classically, whereas the quantum description is necessary at $z < z_0$. The result of calculations appears to be almost independent on the particular value of z_0 for the range of z_0 : 2–4 nm.

From the equations above one can show that the potential $U_{self}(z)$ obeys the following equation for the two-dimensional system under consideration:

$$\frac{dU_{self}}{dz} = -E_{0ext} + \frac{2\pi}{\epsilon} \int dz' [n(z')F(z - z') + n_{fi}(z') \text{sgn}(z - z')], \quad (27)$$

where

$$F(z) = \int \frac{\text{sgn}(z)C(\rho|z|)}{(1 + \rho^2)^{3/2}} \rho d\rho. \quad (28)$$

The electrostatic potential $\varphi(z)$ obeys the equation

$$\frac{d\varphi}{dz} = -E_{0ext} + \frac{2\pi}{\epsilon} \int dz' [n(z') + n_{fi}(z')] \text{sgn}(z - z'), \quad (29)$$

which can be derived from the Poisson equation. The right-hand side of this equation is the actual dc electric field in the subsurface quantum well.

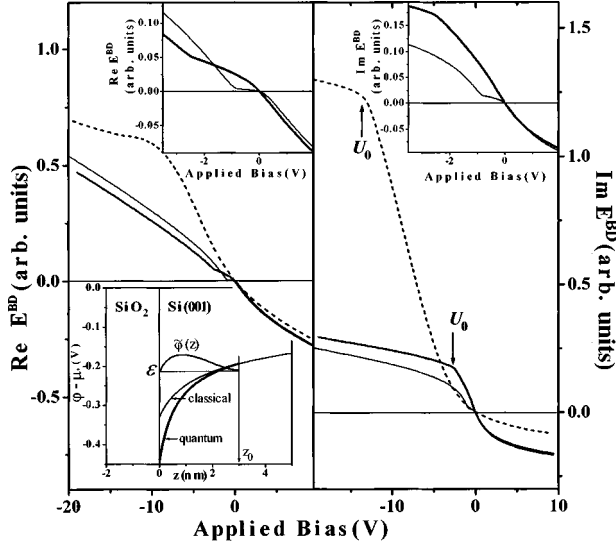


FIG. 2. The bias dependences of the real (left panel) and imaginary (right panel) parts of the EFISH field E^{BD} for three doping levels of an n -Si wafer covered by a 19-nm-thick oxide: $N_D = 10^{15} \text{ cm}^{-3}$ (thin curve), $N_D = 10^{17} \text{ cm}^{-3}$ (thick curve), and $N_D = 5 \times 10^{18} \text{ cm}^{-3}$ (dashed curve). The flatband voltage is assumed to be zero. The top insets show these bias dependences in the vicinity of the zero-point bias. Bottom inset: schematic of potential distribution in the subsurface region calculated for $\varphi_{int} = -0.33 \text{ V}$ within classical (thin line) and Hartree-Fock (thick line) DCF screenings. The wave function $\tilde{\varphi}(z)$ of the first energy state \mathcal{E} is depicted.

Equations (27) and (29) differ one from one another by the factor $F(z)$ in Eq. (27). It can be shown that since $C(r) \rightarrow 1$ at $r \rightarrow \infty$, $F(z) \rightarrow 1$ at $z \rightarrow \infty$. Therefore, the self-consistent potential $U_{self}(z)$ is closely related to $\varphi(z)$. Moreover, remote charge layers contribute equally to $U_{self}(z)$ and $\varphi(z)$. Nevertheless, the electrostatic and self-consistent potentials are distinguished by the role of quantum effects in the electron plasma. The electrostatic potential describes interactions of a charged probe particle with other charges only via the electromagnetic field. The self-consistent potential $U_{self}(z)$ also includes the electron's tendency to "wedge" itself into other electrons and repulse them via the exchange interaction, and therefore differs fundamentally from $\varphi(z)$. This is reflected by the appearance of the correlation function $F(z)$. On the other hand, the EFISH bias dependence is expressed in terms of the classical potential $\varphi(z)$, because the major contribution to the semiconductor optical response comes from *bound* electrons, whereas screening in the semiconductor is caused by *free* carriers. There are no correlation effects between these two different types of particles.

For every value of E_{0ext} using Eqs. (22), (24), and (25) the density of the screening charge in the quantum well is calculated, and then, using Eq. (29), the spatial distribution of the electrostatic potential $\varphi(z)$ for $0 \leq z \leq z_0$ is found. For $z \geq z_0$, $\varphi(z)$ is evaluated within a classical approach with $\varphi(z_0)$ as a parameter. The boundary condition at z_0 delivers the coincidence of $\varphi(z_0)$ calculated within the HF approach with a classical potential. The inset in Fig. 2 shows the spatial distribution of an electrostatic potential $\varphi(z)$ within the classical and HF approaches for a p -type silicon wafer with

$z_0 = 3 \text{ nm}$. The wave function $\tilde{\varphi}(z)$ of the first energy state \mathcal{E} is also sketched. With quantum corrections $\varphi(z)$ varies more sharply, and the subsurface well becomes deeper.

Summarizing this section, we have obtained a set of equations (22), (24), and (25) for the self-consistent potential $U_{self}(z)$, the electron wave function $\psi_i(\mathbf{r})$, and charge the density $n(z)$. These equations describe the screening in the subsurface region $z < z_0$. This approach takes into account quantum effects in the electronic liquid via the factor $F(z)$, which is related to the in-plane correlation function $C(\mathbf{r}_{||} - \mathbf{r}'_{||})$. These effects become important for a large bias voltage. In this case the dc field drops quickly within a very thin layer near the surface, and the semiclassical picture of an electron gas with the local density depending on the local potential is invalid. Quantum calculations describe nonlocal screening in this situation.

D. Model calculations

In this section the model bias dependence of the EFISH intensity is found by numerical integration of the first integral of the Poisson equation and the wave equation. First, the dependence of the EFISH intensity on the doping of the semiconductor is modeled. Then the influence of the parameters of the semiconductor-insulator interface on the amplitude of the EFISH wave is considered. A planar structure consisting of a silicon wafer covered by an oxide film is considered as a test object.

To find the EFISH field E^{BD} for every value of the interface potential, φ_{int} , the spatial distribution of the DCF $E_0(z)$ across the silicon SCR is calculated numerically by solving the first integral of the Poisson equation (7) with the charge densities given by Eqs. (16) and (17). Then, substituting $E_0(z)$ into Eq. (6), the integral

$$I(U) \equiv I_1 + iI_2 = \int_0^{+\infty} E_0(z) \exp[i(k_{2\omega,z} + 2k_{\omega,z})z] dz, \quad (30)$$

is numerically evaluated. The corresponding value of applied bias U is related to the interface field $E_{int} = E_0(z=0_+)$ and the interface potential φ_{int} by

$$U = \epsilon_{sc} \epsilon_d^{-1} E_{int}(\varphi_{int}) D + \varphi_{int}. \quad (31)$$

The EFISH field E^{BD} is a product of the integral $I(U)$ and the complex factor $F_{2\omega} F_{\omega}^2 \chi_{eff}^{BD} = F \exp(i\phi_F)$, which is a bias-independent constant for a given fundamental wavelength. This allows us to consider bias dependences $I_1(U)$ and $I_2(U)$ as bias dependences of $\text{Re } E^{BD}$ and $\text{Im } E^{BD}$ in units of F shifted in the complex frame by an angle of ϕ_F . This notation is used in the numerical experiment shown in Figs. 2, 4, and 5. Figure 2 shows $\text{Re } E^{BD}$ and $\text{Im } E^{BD}$ as functions of the bias applied to a MOS structure consisting of an n -type silicon wafer with dopant concentrations $N_D = 10^{15} \text{ cm}^{-3}$ (thick line), $N_D = 10^{17} \text{ cm}^{-3}$ (thin line) and $N_D = 5 \times 10^{18} \text{ cm}^{-3}$ (dashed line) covered by a silicon oxide film 19 nm thick. The fundamental radiation wavelength is set at 730 nm. The optical constants of silicon have been taken from Ref. 55.

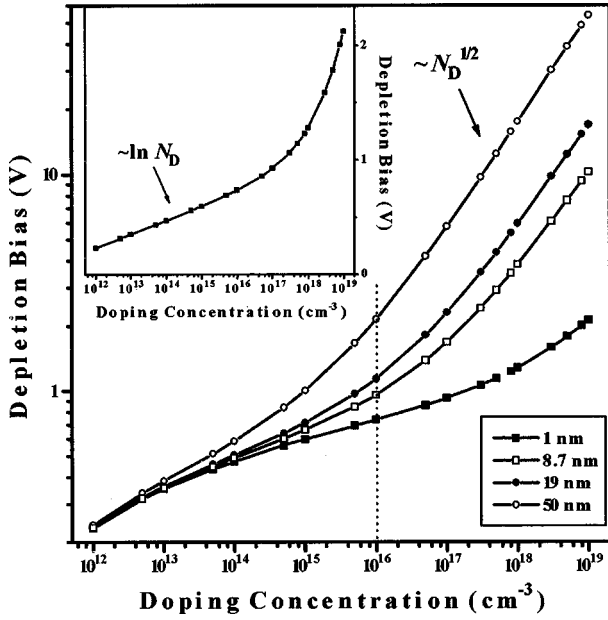


FIG. 3. The absolute value of the depletion bias U_0 vs the doping concentration N_D of the n -Si wafer for Si-SiO₂-metal MOS structures with different SiO₂ thicknesses: 1 nm (filled squares), 8.7 nm (open squares), 19 nm (filled circles), and 50 nm (open circles). Solid curves are guides to the eye. Inset: dependence of $|U_0|$ on N_D for MOS structure with 1-nm-thick oxide on a linear scale.

Two important trends in these curves are noteworthy. First, $\text{Im } E^{BD}$ depends strongly on the bias only in the region of negative biases between 0 V and a saturation bias we denote as U_0 . Outside of this interval $\text{Im } E^{BD}$ saturates. This strongly contradicts the previous phenomenological assumption (and the EFISH intensity quadratically) on the applied bias. The saturation of the imaginary part of the EFISH field amplitude for $U < U_0$ and $U > 0$ is attributed to the inversion and accumulation regimes of external bias screening in the SCR (see the inset in Fig. 1) since the DCF is mostly localized inside a thin subsurface layer of nm-scale thickness. Since the imaginary part of the Green's function is equal to zero exactly at the interface, $\text{Im } E^{BD}$ becomes practically insensitive to the DCF inside the inversion and accumulation layers. Thus $U = U_0$ and $U = 0$ define end points of a bias region which corresponds to the depletion regime; the interface potential φ_0 for external bias U_0 is equal to $2(\varepsilon_i - \mu)$, where ε_i is the midgap energy.⁵⁶

Second, the decrease of the dopant concentration leads to a decrease of the absolute value of U_0 and E^{BD} . Figure 3 shows the dependence of $|U_0|$ on the dopant concentration of the n -type silicon wafer for various oxide thicknesses. For dopant concentrations larger than 10^{16} cm^{-3} , the absolute value of U_0 scales approximately as the square root of N_D , while for smaller doping levels $|U_0|$ scales as $\ln N_D$, as is clearly shown in the inset of Fig. 3. Within the Schottky approximation for the SCR,⁵² the interface potential φ_{int0} and interface field E_{int0} , corresponding to applied bias U_0 , are given by

$$E_{int0} = 2\sqrt{\xi\varphi_{int0}},$$

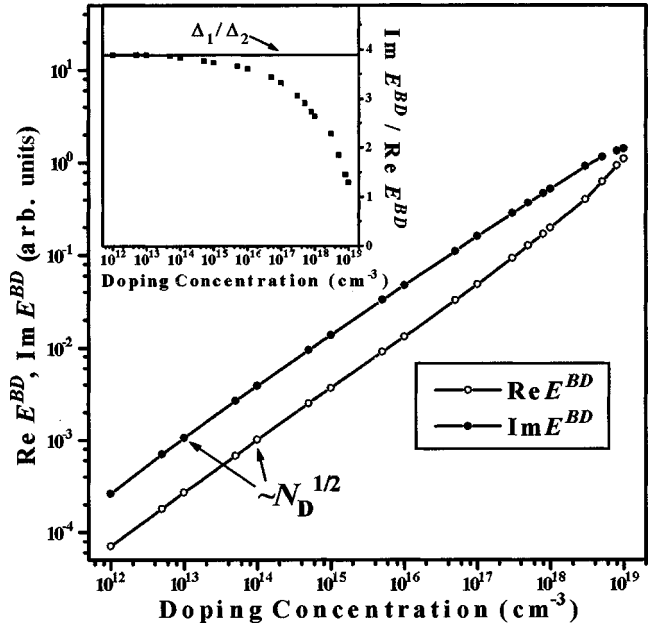


FIG. 4. The real (open circles) and imaginary (filled circles) parts of E^{BD} for the depletion bias U_0 vs the doping concentration N_D of the silicon wafer with a 19-nm-thick oxide film. Solid curves are guides to the eye. Inset: the doping dependence of the ratio of $\text{Im}(E^{BD})/\text{Re}(E^{BD})$.

$$\varphi_{int0} = 2[\varepsilon_i - kT \ln(N_D N_C^{-1})], \quad \xi = 2\pi e N_D \varepsilon_{sc}^{-1}. \quad (32)$$

Applied bias U_0 according to Eq. (31) consists of voltage drops $\varepsilon_{sc} \varepsilon_d^{-1} E_0(\varphi_{int0}) D$ across the oxide film, and φ_{int0} across the silicon SCR. Therefore, for high doping levels the applied bias mostly drops across the oxide layer and $U_0(N_D) \propto E_{int0}(N_D) \propto \sqrt{N_D \ln(N_D N_C^{-1})}$. For low doping levels the interface potential dominates, and $U_0(N_D) \propto \varphi_{int0}(N_D) \propto \ln(N_D N_C^{-1})$. For thinner oxide layers, less of the applied voltage drops across the oxide, and the transition from a logarithmic to a square root doping dependence of U_0 occurs at a higher doping level.

Figure 4 shows the EFISH amplitudes for applied bias U_0 as functions of donor concentration, N_D . Over a wide range of concentrations $\text{Re } E^{BD}$ and $\text{Im } E^{BD}$ are proportional to the square root of N_D . The latter can be explained by integrating Eq. (6) with a linear DCF $E_0(z) = E_{int0} - 2\xi z$ across the SCR, as in the Schottky model. This integration yields the following expressions for the EFISH field:

$$\text{Re } E^{BD} \propto E_{int0} \Delta_2 + 2\xi \frac{\Delta_1^2 - \Delta_2^2}{\Delta_1^2 + \Delta_2^2}, \quad (33)$$

$$\text{Im } E^{BD} \propto E_{int0} \Delta_1 - 4\xi \frac{\Delta_1 \Delta_2}{\Delta_1^2 + \Delta_2^2}, \quad (34)$$

where $\Delta_1 = \text{Re}(2k_\omega + k_{2\omega})$ and $\Delta_2 = \text{Im}(2k_\omega + k_{2\omega})$. Since the interface field $E_{int0} = 2\xi W$ depends linearly on the width of the SCR, the restrictions $W\Delta_1 \gg 1$ and $W\Delta_2 \gg 1$ lead to the following expression for the complex EFISH field: $E^{BD} \propto E_{int0}(\Delta_2 + i\Delta_1) \propto \sqrt{N_D \ln(N_D N_C^{-1})}$. Thus $\text{Re } E^{BD}$ and $\text{Im } E^{BD}$ scale approximately as the square root of N_D . Furthermore, $\text{Im } E^{BD}/\text{Re } E^{BD} = \Delta_1 \Delta_2^{-1}$, i.e., the ratio of $\text{Re } E^{BD}$

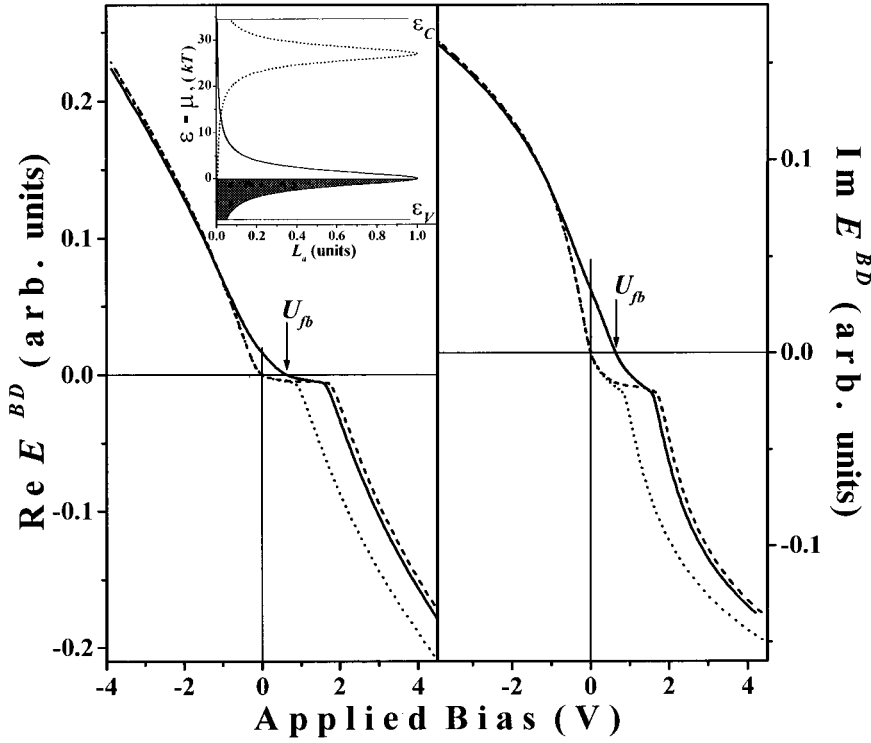


FIG. 5. The bias dependences of the real (left panel) and imaginary (right panel) parts of the EFISH field E^{BD} for different parameters of acceptor interface states calculated for p -silicon covered by an 8.7-nm-thick oxide film. The dotted curves are presented for comparison to the same dependences without traps. The energy spectrum of the interface states is simulated by a Lorentzian function with density $N_a = 2 \times 10^{13}$ traps cm^{-2} eV^{-1} , width $\delta_a = 2kT$, and different central positions $\epsilon_{0a} = \mu$ (thin curves) and $\epsilon_{0a} - \mu = 26kT$ (dashed curves) as depicted on the inset. The filled area in the inset shows the energy interval with charged acceptor traps.

to $\text{Im} E^{BD}$, is the ratio of the characteristic length scale of absorption, Δ_2^{-1} , to that of retardation, Δ_1^{-1} , for the SH waves. Since the energy of the 365-nm SH photon used in our calculations is close to the E_1 critical point of silicon, $\Delta_1 = (1/5.7) \text{ nm}^{-1}$ and $\Delta_2 = (1/21.5) \text{ nm}^{-1}$ are sufficiently large to satisfy the conditions $W\Delta_1 \gg 1$ and $W\Delta_2 \gg 1$ for dopant concentrations up to 10^{18} cm^{-3} (Fig. 4). As shown in the inset of Fig. 4, the ratio $\text{Im} E^{BD}/\text{Re} E^{BD}$ is close to the value of $\Delta_1\Delta_2^{-1} = 3.89$.

E. Role of interface states in the EFISH phenomenon

A sheet of charged interface states changes the relationship between the potential drop across silicon and the applied bias due to the boundary condition for normal components of the electric displacement vector \mathbf{D} . To demonstrate the role of interface traps in the EFISH phenomenon, we consider the distribution of trap levels across the silicon band gap as a set of Lorentz functions. The charge density of interface traps n_{it} , as a function of the interface electrostatic potential, is given by Eq. (18):

$$n_{it}[\varphi(z=0_+)] = e \int_{\epsilon_V}^{\epsilon_C} d\epsilon \sum_M \text{sgn}(n_{it}^M) F^M(\varphi - \epsilon) \times \sum_j N_{M,j} L_{M,j}(\varphi - \epsilon), \quad (35)$$

with

$$L_{M,j}(\epsilon) = \delta_{M,j}^2 [\delta_{M,j}^2 + (\epsilon - \epsilon_{0M,j})^2]^{-1}. \quad (36)$$

Here j numerates Lorentz functions of the energy distribution of the trap levels, $M = a, d$. $N_{M,j}$, $\delta_{M,j}$, and $\epsilon_{0M,j}$ denote the effective density of traps per eV and the width and central positions of the j th Lorentz peak, respectively. These Lor-

entz functions simulate the continuous energy distribution of traps. By setting $\delta_{M,j} \rightarrow 0$, one can account for discrete levels.

Figure 5 shows the bias dependence of $\text{Re} E^{BD}$ and $\text{Im} E^{BD}$ for the MOS structure used in our experiment which is comprised of p -type Si with a donor concentration of $1.5 \times 10^{15} \text{ cm}^{-3}$ and a 8.7-nm-thick thermal SiO_2 layer. Interface traps are presumed to be acceptors with $N_a = 2 \times 10^{13}$ traps cm^{-2} eV^{-1} and $\delta_a = 2kT$. For illustration two different central positions are considered: $\epsilon_{0a} = \mu$ (thin lines) and $\epsilon_{0a} - \mu = 26kT$ (dashed lines). The distribution of such traps across the silicon band gap L_a is sketched at the inset in Fig. 5. The dotted lines are presented for comparison to the same EFISH field components in the absence of traps. For negative biases in the accumulation regime, bands are bent in such a way that all the trap levels are above the Fermi energy, acceptor traps are empty, and the bias dependence of the SH field components is unaffected by the presence of these uncharged traps. As the magnitude of the negative bias is decreased, the bands are bent less, and trap levels begin to fall below the Fermi energy; first the traps with low-energy levels, then those with higher energy. Consequently, the bias dependences of $\text{Re} E^{BD}$ and $\text{Im} E^{BD}$ start to deviate from the dependence for $N_a = 0$, demonstrating the saturationlike feature. This is attributed to the pinning of the Fermi level. As the level of the neutral traps crosses the Fermi energy, the charge density of the interface traps changes, and application of a smaller bias leads to a decrease in the voltage drop across the oxide film while the interface potential and the DCF spatial distribution remain fixed until the trap level is completely filled. For the flatband condition some of the interface traps appear to be charged. The bias dependences of $\text{Re} E^{BD}$ and $\text{Im} E^{BD}$ for $N_a \neq 0$ pass through the EFISH intensity zero-point for a flatband voltage U_{fb} , which depends linearly on the interface charge n_{it} . In the case of donor

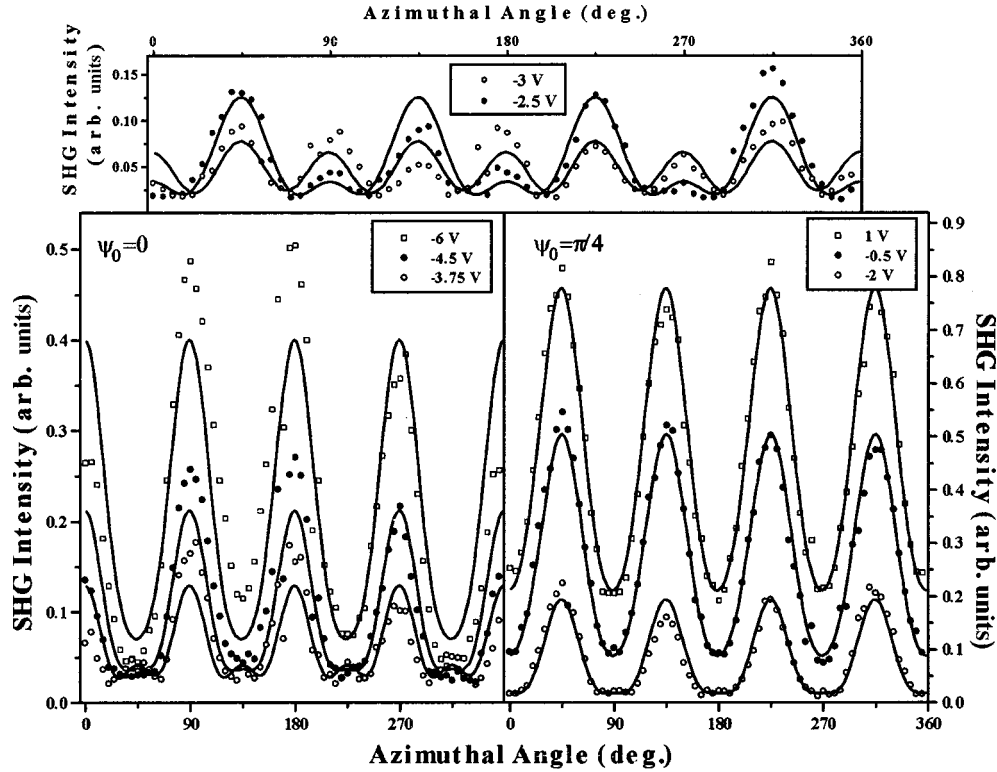


FIG. 6. *p*-in, *p*-out SHG signal from an *n*-Si(001) MOS structure at several biases for $\lambda_\omega = 725$ nm ($2\hbar\omega = 3.43$ eV) vs sample azimuthal angle. Solid curves are fits to data by the zeroth, fourth, and eighth Fourier components.

interface traps the same effects are obtained, but the bias dependences of $\text{Re} E^{BD}$ and $\text{Im} E^{BD}$ for $N_a = 0$ and $N_a \neq 0$ differ in the accumulation regime.

III. RESULTS AND DISCUSSION

A. Experimental

For the EFISH experiments the output of an unamplified Ti:sapphire laser ranging from 710 to 800 nm was used. The Ti:sapphire laser generates 120-fs pulses with an average power of 200–300 mW at a repetition rate of 76 MHz, which is well below the damage threshold of the semiconductor. The *p*-polarized beam was focused onto the sample at a 45° angle of incidence. A reflected *p*-polarized SHG signal was selected by the use of appropriate filters, and directed into a photon-counting system. High-intensity, high-repetition-rate, short pulses provided a good signal-to-noise ratio in our experiments while avoiding significant sample heating. A small split off portion of the fundamental beam was focussed through a *z*-cut quartz crystal that provided a reference SHG signal.

The MOS structures were fabricated from two types of Si(001) wafers: a heavily doped *n*-type (10^{18} cm $^{-3}$, Sb doped) wafer covered by a 19-nm-thick SiO $_2$ film, and a lightly doped *p*-type (1.5×10^{15} cm $^{-3}$, B doped) wafer with a 8.7-nm-thick SiO $_2$ film. A 3-nm semitransparent chromium cap layer, and an Ohmic aluminum backside electrode, were evaporated onto the samples. Single-wavelength ellipsometry was used to measure the SiO $_2$ thicknesses. As an independent calibration of the flatband voltage, spatially resolved surface photovoltage measurements were performed on the same samples. The external bias voltage was applied be-

tween the chromium and aluminum electrodes. The SHG response from the chromium layer was verified to be negligible in comparison with the SHG signal from the buried Si(001)-SiO $_2$ interface.

The bias dependence of the rotational azimuthal anisotropy of the EFISH intensity was measured over a wide range of the bias voltages at various fundamental wavelengths from 710 to 800 nm. Figure 6 shows the azimuthal dependence of the EFISH intensity measured for an *n*-Si(001) MOS structure. The pronounced fourfold-symmetric anisotropy of the EFISH intensity riding on a significant isotropic (independent of the azimuthal angle) background was observed at most biases. Variations in the applied voltage change the amplitude of both the fourfold-symmetric and isotropic contributions, both of which increase with increasing the absolute value of the bias. At the center of the applied bias region near -2.75 V (upper panel), the azimuthal dependence possesses a significant eightfold-symmetric component, which appears to be comparable with isotropic and fourfold components for the same bias. As the applied voltage passes through this value the azimuthal dependences shift by $\pi/4$. Similar features of the field-induced rotational anisotropy were observed throughout the studied spectral range. Figure 7 shows the azimuthal dependence for a *p*-Si MOS structure which demonstrates similar behavior, except that the eightfold-symmetric component is observed at -1.2 V, and the isotropic component was much larger than the fourfold component.

B. EFISH at Si(001)-SiO $_2$ interface: role of the spatial DCF distribution

The azimuthal angular dependence of the SHG intensity from the Si(001)-SiO $_2$ interface in the presence of the DCF

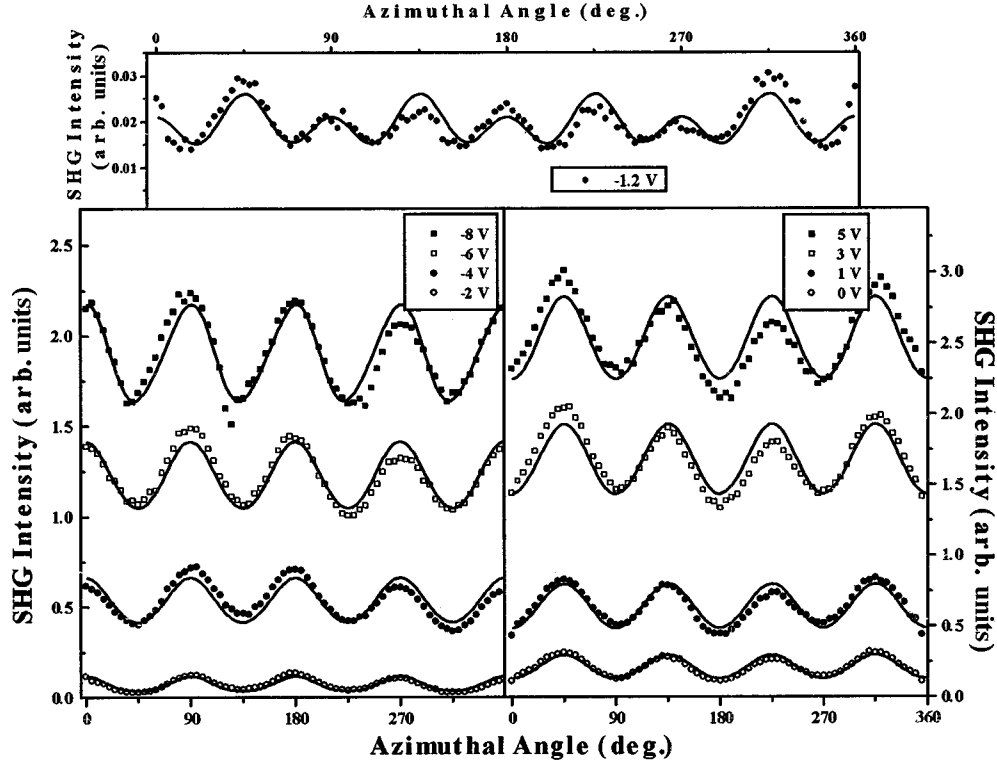


FIG. 7. *p*-in, *p*-out SHG signal from a *p*-Si(001) MOS structure at several biases for $\lambda_\omega = 730$ nm ($2\hbar\omega = 3.41$ eV) as a function of sample azimuthal angle. Solid curves are fits to data by the zeroth, fourth, and eighth Fourier components.

can be described phenomenologically as optical interference of dc-field-dependent, isotropic, and dc-field-independent, fourfold-symmetric, components of the SH field:²⁰

$$\begin{aligned}
 I_{2\omega}(\psi, V) &= |a(V) + b \cos[4(\psi - \psi_0)]|^2 \\
 &= c_0(V) + c_4(V) \cos[4(\psi - \psi_0)] \\
 &\quad + c_8 \cos[8(\psi - \psi_0)], \quad (37)
 \end{aligned}$$

where ψ_0 is the azimuthal angle of a maximum of rotational anisotropy, and a and b are the amplitudes of the isotropic and anisotropic components of the SH field, respectively. The surface, \mathbf{P}^S , and the bulk DCF-induced, \mathbf{P}^{BD} , components of the nonlinear polarization \mathbf{P}^{NL} contribute to the isotropic component a while the fourfold-symmetric component b originates from the bulk quadruple polarization \mathbf{P}^{BQ} .⁴⁷ For the sake of simplicity we take the amplitude b of the fourfold-symmetric anisotropic component as a real quantity, and define the phase of the isotropic component $a = a' + ia''$ with respect to b . As a result the dependence of the EFISH intensity on the azimuthal angle, ψ , is given by a Fourier expansion [Eq. (37)] with zeroth, fourth, and eighth Fourier components:

$$c_0 = a'^2 + a''^2 + \frac{1}{2}b^2, \quad c_4 = 2a'b, \quad c_8 = \frac{1}{2}b^2. \quad (38)$$

The fourth Fourier component c_4 , which is an interferometric cross-term between surface and DCF-induced SHG contributions, can be considered as a homodyne detection of a DCF-induced SH field using internal (surface field independent) reference signal.⁴⁵ In this way, the c_4 Fourier component of the EFISH intensity is linear proportional to the electric field E^{BD} and, therefore, sensitive to the sign of E^{BD} .

Figure 8 shows the bias dependence of the isotropic Fourier component of the EFISH intensity (left panel) and of the normalized fourfold Fourier component $c_4(2\sqrt{2}c_8)^{-1}$ (right panel), which is exactly the a' component of the EFISH field, extracted from azimuthal dependences for *n*-Si MOS structure in Fig. 6. The error bars are the averaged amplitudes of Fourier components c_1 and $c_3(2\sqrt{2}c_8)^{-1}$, respectively. Although the eightfold-symmetric component c_8 is significantly smaller than the fourfold term, it is quite distin-

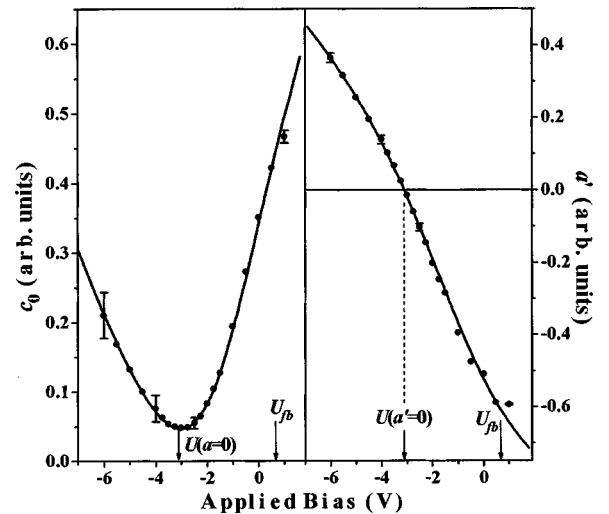


FIG. 8. Bias dependences of isotropic c_0 and normalized fourfold $a' = c_4(2\sqrt{2}c_8)^{-1}$ SHG Fourier amplitudes for *n*-Si(001) MOS structure for $\lambda_\omega = 725$ nm ($2\hbar\omega = 3.43$ eV). Solid curves are fits to data using the model presented.

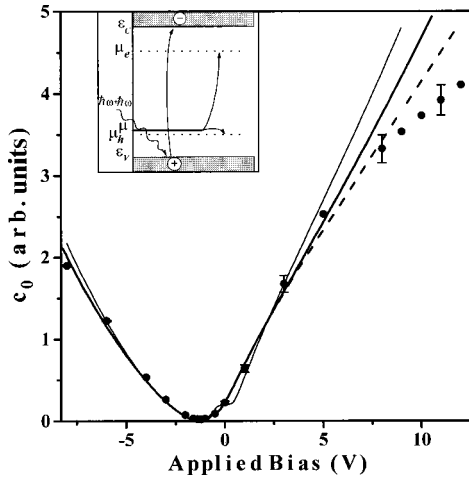


FIG. 9. The isotropic SHG component from a p -Si(001) MOS structure for $\lambda_\omega = 730$ nm ($2\hbar\omega = 3.41$ eV) as a function of applied bias. Curves are fits to data using the model of the DCF screening within the classical approach with $N_A = 1.5 \times 10^{15}$ cm $^{-3}$ (thin curve), within the quasiequilibrium approximation with $\mu_e = \epsilon_C - 0.22$ eV and $\mu_h = \epsilon_V + 0.19$ eV (thick curve), and with surface quantization corrections (dashed curve). The inset shows a diagram of the Fermi-level splitting due to two-photon absorption and generation of e - h pairs.

guishable for all biases and at least an order of magnitude larger than neighboring noise c_7 and c_9 Fourier components. The eightfold-symmetric SHG component c_8 appears to be field independent throughout the range of applied biases, consistently with model assumptions [Eqs. (37) and (38)]. The component $c_0(U)$ is almost a quadratic function of applied bias U with a minimum at -3.1 V. The a' component also passes through a zero point at approximately -3.1 V, and depends on bias almost linearly with pronounced deviations from linearity at the edges of the bias range. The bias dependences $c_0(U)$ and $a'(U)$ are simultaneously fitted by the model curve $I(U)$, which has been calculated by integrating Eq. (30) for a dopant concentration of 5×10^{18} cm $^{-3}$, and is shown in Fig. 2 by a dashed line. Adjustable fit parameters are the field-independent part of a , the flatband voltage U_{fb} , and the phase ϕ_F . The solid curves in Fig. 8 show the results of an approximation with $U_{fb} = 0.7$ V which agree well with the experimental data. The obtained value of the flatband voltage significantly differs from either the minimum of $c_0(U)$ or the bias for which $a' = 0$. This difference is attributed to the optical interference of the DCF-dependent (bulk) and DCF-independent (surface) contributions to a . For this highly doped MOS structure the entire 8-V range of applied biases corresponds to the depletion regime, and surface quantization effects are not important.

For a p -Si MOS structure the eightfold component is observable only for the bias region around -1.2 V, where ψ_0 in Eq. (37) shifts by $\pi/4$. However, based on its bias independence, the mean value of c_8 was used for normalization of c_4 term. Figures 9 and 10 show the bias dependence of c_0 and a' for the p -Si MOS structure extracted from azimuthal dependences presented in Fig. 7. The quasiquadratic behavior of $c_0(U)$ with a minimum at -1.25 V, and the approximately linear dependence of $a'(U)$ with deviations at the limits, are similar to the trends of the n -Si MOS structure.

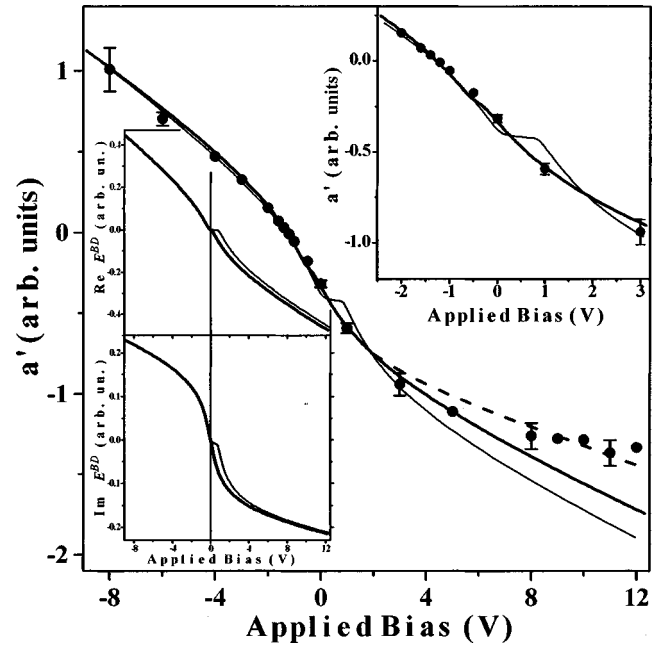


FIG. 10. The normalized fourfold-symmetric SHG component $a' = c_4(2\sqrt{2}c_8)^{-1}$ for a p -Si(001) MOS structure for $\lambda_\omega = 730$ nm ($2\hbar\omega = 3.41$ eV) as a function of applied bias. Curves are fits to data using the model of the DCF screening within the classical approach with $N_A = 1.5 \times 10^{15}$ cm $^{-3}$ (thin curve), within the quasiequilibrium approximation with $\mu_e = \epsilon_C - 0.22$ eV and $\mu_h = \epsilon_V + 0.19$ eV (thick curve), and with surface quantization corrections (dashed curve). Top inset: voltage dependences near the zero point of the bias. The bottom insets show the model bias dependences of the EFISH field complex amplitude for a p -Si MOS structure with a 8.7-nm-thick oxide film and $N_A = 1.5 \times 10^{15}$ cm $^{-3}$ calculated within the classical approach to the DCF screening (thin lines), and using the model of the Fermi-level splitting.

Thin lines in Figs. 9 and 10 show the fit to the experimental data. The model bias dependences $I_1(U)$ and $I_2(U)$, calculated for a dopant concentration of 1.5×10^{15} cm $^{-3}$, are depicted in the insets in Fig. 10 by thin lines. The approximation shows a clear steplike feature near the center bias which corresponds to the depletion regime of the SCR in p -type silicon. However, such a peculiarity has not been observed experimentally. This discrepancy between the model and experiment occurs for calculations including surface quantization as well (Sec. II C), because at these small biases the surface-quantization effects are negligible.

One possible explanation for the experimentally measured bias dependences is the effect of photoexcited carriers on EFISH. The absorption of femtosecond laser pulses leads to the excitation of electron-hole (e - h) pairs in the SCR. The DCF in the SCR separates these photoexcited carriers, and the density of the charge injected into the SCR for a pulse duration of $\tau \sim 120$ fs and a fluence of fundamental radiation of about 10^{-5} J/cm $^{-2}$ can be up to 10^{17} cm $^{-3}$.⁶ A systematic description of the influence of photoexcited carriers on the DCF screening requires a model that rigorously accounts for the kinetics of electron-hole recombination in the subsurface layer. As the e - h thermalization time τ_E is much smaller than carrier recombination times τ_e and τ_h , carrier injection can be described using a quasiequilibrium approximation.⁵⁷ The total density of carriers, including photoexcited e - h

pairs, is given by equilibrium expressions (16) replacing Fermi level μ with quasi-Fermi levels μ_e and μ_h for electrons and holes, respectively (see the inset of Fig. 9). Splitting the initial Fermi level μ into μ_e and μ_h can be effectively taken into account as a presence of compensated donor and acceptor dopants with densities $N_D^* = N_A^*$ such that $\mu_e = \varepsilon_C - kT \ln[N_C(N_D^*)^{-1}]$ and $\mu_h = \varepsilon_V + kT \ln[N_V(N_A + N_A^*)^{-1}]$. For an approximation of bias dependences $c_0(U)$ and $a^1(U)$, the concentration of compensated dopant was varied in the interval of 10^{14} – 10^{17} cm^{-3} . The best agreement of the model with experimental data is achieved for $U_{fb} = -0.55$ V and $N_D^* = N_A^* = 5 \times 10^{15}$ cm^{-3} , that corresponds to $\varepsilon_C - \mu_e = 0.22$ eV and $\mu_h - \varepsilon_V = 0.19$ eV. The corresponding fitting curves are presented in Figs. 9 and 10 by thick lines. Thick lines at the insets in Fig. 10 show the model bias dependences $\text{Re} E^{BD}$ and $\text{Im} E^{BD}$ used for this fit. The thin lines are presented for comparison to the same EFISH field components in the absence of compensated dopants. Carrier injection leads to drastic changes for the bias interval corresponding to the depletion regime of DCF screening, while in the inversion regime bias dependences of EFISH field components are insensitive to this effect. In depletion the external dc field is screened by ionized dopants. In the case of the photogeneration of carriers in the SCR with a density comparable to the dopant concentration N_A , the dc field is mostly screened by minority carriers as in inversion regime. Therefore, due to photoinjection of e - h pairs, the depletion regime can disappear completely.

For biases larger than 4 V, which corresponds to the strong inversion regime, clear deviations of the model from experimental data are observed. This is attributed to the strong localization of the DCF inside a very thin subsurface layer where the bulk description of the DCF screening is not expected to be valid, and one should take surface quantization effects into account. The dashed curve shows the approximation of the data by the model with quantum corrections (Sec. II C) which demonstrates better agreement with experimental data points in this bias region.

C. EFISH spectroscopy: Bulk origin of the dc field-induced contribution

Tuning the fundamental wavelength in the vicinity of the direct two-photon E_1 transition allows measurement of the spectrum of the EFISH intensity and deconvolution of the bulk and surface contributions to the SHG signal.^{9,11,58,59} Figure 11 shows the bias dependence $c_4(U)$ for various wavelengths of the fundamental radiation, λ_ω . Tuning of λ_ω from 800 nm to the two-photon resonance near 3.4 eV ($\lambda_\omega = 730$ nm) produces a stronger bias dependence for both $c_4(U)$ and $c_0(U)$. Further decrease of λ_ω results in a reduction of this bias dependence. The bulk quadrupole component of the SH field, $b \equiv E_{anis}^{BQ}$, contributes to both the isotropic, c_0 , and fourfold-symmetric, c_4 , Fourier components. To extract the spectral dependence of the EFISH field, E^{BD} , one must find the spectrum of $|E_{anis}^{BQ}|$. The latter is obtained from the spectrum of the eighth Fourier component, c_8 , averaged over the entire bias region. Integration of the product of the Green's function and the bulk quadrupole polarization, according to Eq. (5), gives the spectral behavior of $|E_{anis}^{BQ}|$ in the form

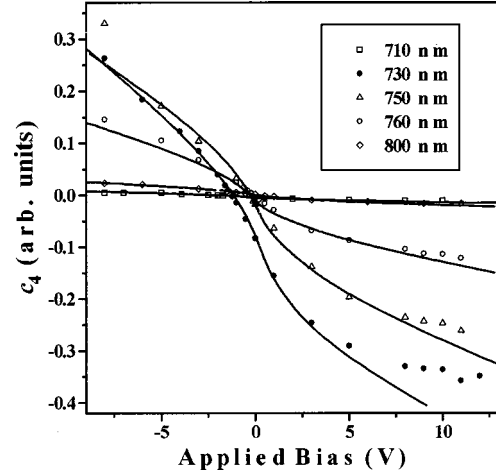


FIG. 11. The bias dependences of the fourfold-symmetric anisotropic SHG component $c_4(U)$ for five wavelengths of the fundamental radiation, and their fits presented by solid lines.

$$|E_{anis}^{BQ}(\Omega)| = I_\omega \left| \frac{k_{\omega,z}^2(\Omega)}{k_{2\omega,z}(\Omega) + 2k_{\omega,z}(\Omega)} \right| \times |F_\omega^2(\Omega) F_{2\omega}(\Omega)| |\chi^{(2),BQ}(\Omega)|. \quad (39)$$

We denote $|\chi^{(2),BQ}(\Omega)|$ as the magnitude of a combination of $\chi^{(2),BQ}$ tensor components responsible for the fourfold-symmetric part of \mathbf{P}^{BQ} . I_ω is the fundamental intensity. Figure 12 shows the spectrum of the magnitude of the effective quadrupole susceptibility $|\chi^{(2),BQ}(\Omega)|$. The filled symbols in Fig. 12 show the spectral dependence of the effective cubic susceptibility $\chi^{(3),BD}$ extracted from the set of bias dependences $c_0(V, \lambda)$. The spectra of both $|\chi^{(2),BQ}(\Omega)|$

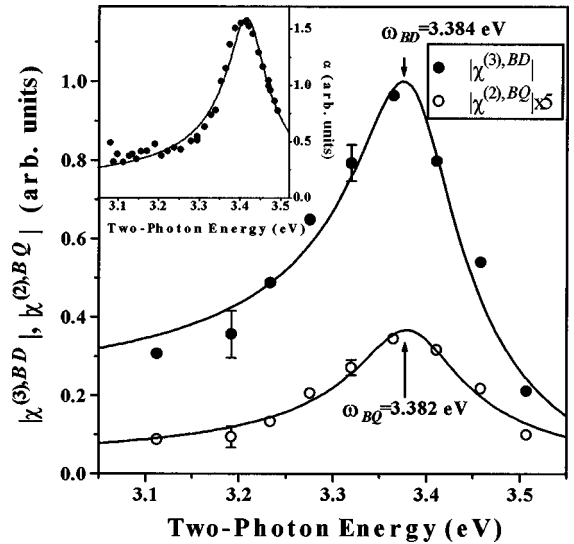


FIG. 12. The spectral dependence of the cubic dipole and quadratic quadrupole susceptibilities in the vicinity of the direct two-photon E_1 transition extracted from the spectra of the EFISH azimuthal dependences. Solid lines are fits to data by the Lorentz function with a real background. Inset: the spectral dependence of the efficiency of modulated EFISH for $\Delta U = 0.6$ V and $\Omega = 100$ Hz in a p -Si(001) MOS structure.

TABLE I. Spectral parameters of $|\chi^{(2),BQ}(\Omega)|$ and $|\chi^{(3),BD}(\Omega)|$.

	α , rel.un.	β , rel.un.	δ , eV	ω_M , eV
<i>BQ</i>	-0.005	0.006	0.054	3.382
<i>BD</i>	-1.216	0.378	0.053	3.384

and $|\chi^{(3),BD}(\Omega)|$ peak at approximately 3.4 eV, and have been fitted by a single Lorentz function with a real constant background

$$\chi^M(\Omega) = \alpha + \frac{\beta}{\Omega - \omega_M + i\delta}, \quad (40)$$

with $M=BQ, BD$. The solid curves in Fig. 12 show the spectral fits of $|\chi^{(2),BQ}(\Omega)|$ and $|\chi^{(3),BD}(\Omega)|$ by Eq. (40) with the parameters presented in Table I. The values of resonance positions obtained are shown to be close to 3.38 eV. This is consistent with the energy of the bulk E_1 critical point as known from linear spectroscopy, and fully indicates a bulk origin of the EFISH response.

D. Low-frequency electromodulation SHG spectroscopy of the Si(001)-SiO₂ interface

Modulation techniques are widely used in optical spectroscopy⁶⁰ because of their sensitivity. Microwave frequency and pulse-voltage modulation of the SHG response in Si-based MOS structures were studied in Refs. 40 and 34, respectively. Low-frequency electromodulation SHG from a GaN surface in an electrochemical cell was studied in Ref. 32. The upper panel of Fig. 13 shows the schematic of the low-frequency electromodulation of the SHG signal from the Si-SiO₂ interface in a MOS structure by the application of the superposition of a dc bias U and a low-frequency square-wave modulation voltage $\Delta U(\Omega)$ with amplitude ΔU and frequency Ω . The efficiency of the modulated SHG signal at a certain dc bias U is a relative increment of the EFISH intensity $\Delta I_{2\omega}(U) = I_{2\omega}^+ - I_{2\omega}^-$ with $I_{2\omega}^+ = I_{2\omega}(U + \Delta U)$ and $I_{2\omega}^- = I_{2\omega}(U - \Delta U)$ while applying the modulation voltage $\Delta U(\Omega)$. $\Delta I_{2\omega}$ is a measure of the derivative of the EFISH intensity $dI_{2\omega}/dU$, and appears to be a differential characteristic of the EFISH phenomenon which is complementary to the static EFISH dependence $I_{2\omega}(U)$.

The lower panel of Fig. 13 shows the experimental bias dependence of the EFISH increment $\Delta I_{2\omega}$ measured at a *p*-Si(001) MOS structure for $\Delta U = 0.6$ V, $\Omega = 100$ Hz, and $\lambda_{\omega} = 730$ nm at an azimuthal angle $\psi = 0$ that minimizes the anisotropic EFISH intensity. The EFISH increment $\Delta I_{2\omega}$ as a function of bias demonstrates, especially for positive biases, clear deviations from linear behavior which can be expected in the case of a parabolic dependence of $I_{2\omega}$ vs U . Note that these deviations are much more pronounced than nonquadratic features of the bias dependence of $c_0(U)$ (Fig. 9), which indicates the increased sensitivity of EFISH modulation. The static EFISH intensity bias dependence $I_{2\omega}(U)$ and the corresponding half-sum of modulated EFISH intensities $I_{2\omega}^{mod} = 1/2(I_{2\omega}^+ + I_{2\omega}^-)$ are presented in the upper panel of Fig. 13, and show pronounced differences. The most significant differences are seen for negative biases $U < -0.5$,

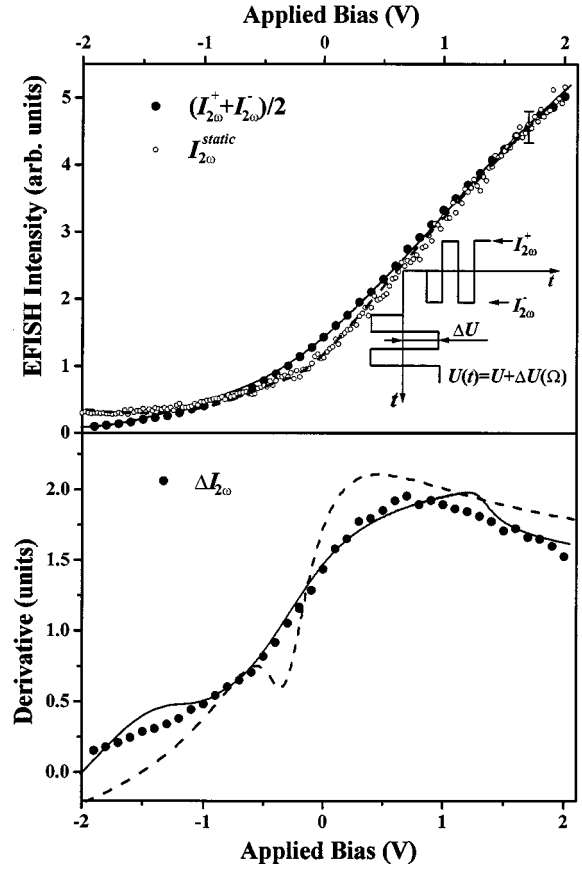


FIG. 13. Static (open circles) and electromodulated (filled circles) bias dependences of the EFISH intensities $I_{2\omega}$ and $I_{2\omega}^{mod}$ (top panel) and of the EFISH intensity increment $\Delta I_{2\omega}$ (bottom panel). The solid and dashed lines show the results of the best fit of the experimental data for electromodulation and static bias applications, respectively. The top panel shows the schematic of the low-frequency electromodulation of the SHG signal by the application of the superposition of dc bias, U , and low-frequency square-wave modulation voltage, $\Delta U(\Omega)$, with amplitude ΔU and frequency Ω .

where $I_{2\omega}(U)$ and $I_{2\omega}^{mod}(U)$ cross, and for positive biases $U > 1.5$, where $I_{2\omega}^{mod}(U)$ starts to saturate. For the central bias region these dependences are nearly parallel. Note that the minimum of $I_{2\omega}(U)$ is reached at -1.7 V, while $I_{2\omega}^{mod}(U)$ does not reach a minimum within the bias region used.

These differences in bias dependences of static and modulated EFISH intensities can be explained by the influence of traps (interface states), located at or near the Si-SiO₂ interface, with a charge dependent on the interface potential. For static EFISH all traps participate in DCF screening, while for electromodulated EFISH intensities $I_{2\omega}^+$ and $I_{2\omega}^-$, interface states with a characteristic trap charging time $\tau_{it} > \Omega^{-1}$ remain neutral and do not change the DCF spatial distribution in the SCR. $I_{2\omega}(U)$ and $I_{2\omega}^{mod}(U)$ and their derivatives $dI_{2\omega}/dU$ and $\Delta I_{2\omega}(U)$, are fitted simultaneously in the framework of the phenomenological model presented in Secs. II A and II D. For static bias application we assume that energy levels of traps are spread over the whole band gap, and interface traps change only the flatband voltage value. At the same time, the levels of slow interface traps are assumed to be localized in a specific region of the band gap. For pulse voltage application the neutrality of slow traps is simulated

as a presence of extra traps of the opposite type, with a Lorentzian distribution across the band gap. The charge density of interface traps, n_{it} , as a function of interface potential is given by Eq. (35), with $N_{a(d)}$, $\delta_{a(d)}$, and $\varepsilon_{0a(d)}$ as adjustable parameters. The results of the best fit are presented in Fig. 13 by solid and dashed lines for pulsed and static bias applications, respectively. The fit has been done for a compensated dopant concentration of $N_D^* = N_A^* = 5 \times 10^{15} \text{ cm}^{-3}$ and a silicon oxide thickness of 8.7 nm. For $I_{2\omega}(U)$ the flatband voltage appears to be -0.55 V . The best fit for $I_{2\omega}^{mod}(U)$ is achieved for an *absence* of donor interface traps with density $N_d = 2 \times 10^{13} \text{ traps cm}^{-2} \text{ eV}^{-1}$, $\delta_d = 2kT$, and $\varepsilon_{0d} = \mu_e$.

The inset in Fig. 12 shows the spectral dependence of the modulation efficiency $\alpha = \Delta I_{2\omega} / I_{2\omega}^{mod}$ in the tuning region of the Ti:sapphire laser. A peak in the spectrum $\alpha(\lambda_\omega)$ is observed at the two-photon energy $2\hbar\omega = 3.41 \text{ eV}$, with a half-width $\hbar\Delta\omega = 0.023 \text{ eV}$. The spectral position of this peak is close to the bulk E_1 resonance. This confirms once again the bulk origin of the DCF-induced term of the nonlinear polarization in Eqs. (1) and (2). The spectral half-width of the resonance in the differential response $\alpha(\lambda_\omega)$ is smaller than the half-width of the resonances of the electrostatic (DCF-induced) EFISH terms in Fig. 12.

Finally, the observed features of electromodulated EFISH response can qualitatively be explained by the influence of interface traps with different charging times. Further comparison of EFISH and $C-V$ data are being performed in order to develop the EFISH electromodulation technique as a real-time and comprehensive probe of interface traps.

IV. CONCLUSIONS

In summary, the dc-electric-field-induced SHG and the low-frequency electromodulation SHG spectroscopy of Si(001)-SiO₂ interfaces in p - and n -type Si(001)-SiO₂-Cr MOS structures have been studied. The dependence of the dc-electric-field-induced SHG intensity on the applied bias is shown to be sensitive to the doping concentration of silicon, the oxide thickness, and the fundamental and SHG wavelengths. From spectroscopy of the anisotropic EFISH dependences the field-induced contribution has been extracted, and the spectrum of the cubic susceptibility $\chi^{(3)}$ appears to be peaked at the energy of the bulk E_1 critical point. The presence of a significant EFISH contribution at an unbiased

Si(001)-SiO₂ interface due to the initial band bending has been observed. This initial band bending contribution should be taken into account in the further interpretation of the spectroscopic SHG measurements at Si(001)-SiO₂ interfaces.^{9,58}

A general phenomenological model of the EFISH phenomenon has been developed. This includes a comprehensive analysis of the generation and the propagation of the EFISH wave in the silicon space-charge region, taking into consideration the retardation and absorption effects, optical interference of multiple reflections in the oxide layer, and interference of the dc-field-dependent and dc-field-independent contributions to the SH waves. The latter interference effect is considered as an *internal homodyne* amplifier of the EFISH contribution to the total SHG response. The spatial distribution of the dc-field-induced bulk dipole nonlinear polarization has been modeled using a rigorously calculated DCF distribution across the SCR, taking surface quantization effects into account. The influences of the silicon doping level, oxide thickness, interface states, and oxide charge traps on the screening of the external DCF in the SCR have been studied. We have demonstrated the sensitivity of the EFISH probe to the charge characteristics of the Si(001)-SiO₂ interface, which makes this technique promising as a noninvasive sensor for the mapping of interface charge distributions in MOS devices.

ACKNOWLEDGMENTS

We are grateful to J. K. Lowell, H. van Driel, T. F. Heinz, G. Lüpke, U. Höfer, W. Daum, J. F. McGilp, A. Yodh, H. W. K. Tom, and K. Pedersen for valuable discussions. This work was supported by the U.S. AFOSR (Contract No. F49620-95-C-0045), the Robert Welch Foundation (Grant No. F-1038), the Texas Advanced Technology Program (Grant No. ATPD-178), and the U.S. National Science Foundation Science and Technology Center Program (Grant No. CHE-8920120), INTAS-93 Grant No. 0370(ext), INTAS Grants Nos. YSF-7, YSF-9, and YSF-10, ISSEP Grants Nos. d98-701 and d98-1012, special Grant No. 96-15-96420 from the Russian Foundation of Basic Research (RFBR) for the Leading Russian Scientific Schools, RFBR Grants Nos. 97-02-17919 and 97-02-17923, Russian Federal Integration Program "Center of Fundamental Optics and Spectroscopy" and Program of the Russian Ministry of Science, "Physics of Solid State Nanostructures."

*Electronic address: aktsip@astral.ilc.msu.su. URL: <http://kali.ilc.msu.su>

†Present address: Department of Physics and Department of Chemistry, Columbia University, New York, NY 10027-6902

¹T. F. Heinz, in *Nonlinear Surface Electromagnetic Phenomena*, edited by H.-E. Ponath and G. I. Stegeman (North Holland, Amsterdam, 1991), p. 355.

²J. F. McGilp, *Prog. Surf. Sci.* **49**, 1 (1995).

³R. M. Corn and D. A. Higgins, *Chem. Rev.* **94**, 107 (1994); G. L. Richmond, J. M. Robinson, and V. L. Shannon, *Prog. Surf. Sci.* **28**, 1 (1988).

⁴N. Bloembergen and Y. R. Shen, *Phys. Rev.* **141**, 298 (1966).

⁵Y. R. Shen, *Surf. Sci.* **299/300**, 551 (1994).

⁶J. I. Dadap, P. T. Wilson, M. H. Anderson, M. C. Downer, and M.

ter Beek, *Opt. Lett.* **22**, 901 (1997).

⁷A. Nahata, J. A. Misewich, and T. F. Heinz, *Appl. Phys. Lett.* **69**, 746 (1996).

⁸J. Bloch, J. G. Mihaychuk, and H. M. van Driel, *Phys. Rev. Lett.* **77**, 920 (1996).

⁹W. Daum, H.-J. Krause, U. Reichel, and H. Ibach, *Phys. Rev. Lett.* **71**, 1234 (1993).

¹⁰K. Pedersen and P. Morgen, *Phys. Rev. B* **52**, R2277 (1995).

¹¹C. Meyer, G. Lüpke, U. Emmerichs, F. Wolter, H. Kurz, C. H. Bjorkman, and G. Lucovsky, *Phys. Rev. Lett.* **74**, 3001 (1995).

¹²B. S. Mendoza and W. L. Mochan, *Phys. Rev. B* **53**, R10 473 (1996); B. S. Mendoza, A. Gaggiotti, and R. Del Sole, *Phys. Rev. Lett.* **81**, 3781 (1998).

¹³C. H. Bjorkman, C. E. Shearon, Y. Ma, T. Yasuda, G. Lucovsky,

- U. Emmerichs, C. Meyer, K. Leo, and H. Kurz, *J. Vac. Sci. Technol. B* **11**, 1521 (1993).
- ¹⁴J. I. Dadap, B. Doris, Q. Deng, M. C. Downer, J. K. Lowell, and A. C. Diebold, *Appl. Phys. Lett.* **64**, 2139 (1994).
- ¹⁵T. F. Heinz, M. M. T. Loy, and W. A. Thompson, *Phys. Rev. Lett.* **54**, 63 (1985).
- ¹⁶O. A. Aktsipetrov, I. M. Baranova, and E. D. Mishina, *Dokl. Akad. Nauk SSSR* **296**, 1348 (1987) [*Sov. Phys. Dokl.* **32**, 839 (1987)].
- ¹⁷P. Bratu and U. Höfer, *Phys. Rev. Lett.* **74**, 1625 (1995).
- ¹⁸J. I. Dadap, Z. Xu, X. F. Hu, M. C. Downer, N. M. Russell, J. G. Ekerdt, and O. A. Aktsipetrov, *Phys. Rev. B* **56**, 13 367 (1997); Z. Xu, X. F. Hu, D. Lim, J. G. Ekerdt, and M. C. Downer, *J. Vac. Sci. Technol. B* **15**, 1059 (1997).
- ¹⁹J. Qi, M. S. Yeganeh, I. Koltover, A. G. Yodh, and W. M. Theis, *Phys. Rev. Lett.* **71**, 633 (1993).
- ²⁰J. I. Dadap, X. F. Hu, M. H. Anderson, M. C. Downer, J. K. Lowell, and O. A. Aktsipetrov, *Phys. Rev. B* **53**, 7607R (1996).
- ²¹O. A. Aktsipetrov, A. A. Fedyanin, and M. C. Downer, in *Notions and Perspectives of Nonlinear Optics*, edited by O. Keller, Series in Nonlinear Optics Vol. 3 (World Scientific, Singapore, 1996), p. 301.
- ²²C. H. Lee, R. K. Chang, and N. Bloembergen, *Phys. Rev. Lett.* **18**, 167 (1967).
- ²³C. K. Chen, A. R. B. de Castro, and Y. R. Shen, *Phys. Rev. Lett.* **46**, 145 (1981).
- ²⁴O. A. Aktsipetrov, E. D. Mishina, and A. V. Petukhov, *Pis'ma Zh. Éksp. Teor. Fiz.* **37**, 592 (1983) [*JETP Lett.* **37**, 707 (1983)].
- ²⁵O. A. Aktsipetrov and E. D. Mishina, *Dokl. Akad. Nauk SSSR* **274**, 65 (1984) [*Sov. Phys. Dokl.* **29**, 37 (1984)].
- ²⁶O. A. Aktsipetrov, I. M. Baranova, L. V. Grigor'eva, K. N. Evtyukhov, E. D. Mishina, T. V. Murzina, and I. V. Chernyi, *Kvant. Elektron. (Moscow)* **18**, 943 (1991) [*Sov. J. Quantum Electron.* **21**, 854 (1991)].
- ²⁷O. A. Aktsipetrov, I. M. Baranova, K. N. Evtyukhov, T. V. Murzina, and I. V. Chernyi, *Kvant. Elektron. (Moscow)* **19**, 869 (1992) [*Sov. J. Quantum Electron.* **22**, 807 (1992)].
- ²⁸P. R. Fischer, J. L. Daschbach, and G. L. Richmond, *Chem. Phys. Lett.* **218**, 200 (1994).
- ²⁹J. L. Daschbach, P. R. Fischer, D. E. Gragson, D. Demarest, and G. L. Richmond, *J. Phys. Chem.* **99**, 3240 (1995).
- ³⁰O. A. Aktsipetrov, I. M. Baranova, L. L. Kulyuk, A. V. Petukhov, E. K. Arushanov, A. A. Shtanov, and D. A. Shutov, *Fiz. Tverd. Tela (Leningrad)* **28**, 3228 (1986) [*Sov. Phys. Solid State* **28**, 1822 (1986)].
- ³¹O. A. Aktsipetrov, I. M. Baranova, and L. L. Kulyuk, in *Proceedings of ICONO-13* (Russian Academy of Sciences, Minsk, Russia, 1988), Vol. 1, p. 15.
- ³²J. Miragliotta and D. K. Wickenden, *Phys. Rev. B* **53**, 1388 (1996).
- ³³J. M. Lantz and R. M. Corn, *J. Phys. Chem.* **98**, 4899 (1994).
- ³⁴O. A. Aktsipetrov, A. A. Fedyanin, V. N. Golovkina, and T. V. Murzina, *Opt. Lett.* **19**, 1450 (1994).
- ³⁵O. A. Aktsipetrov, A. A. Fedyanin, E. D. Mishina, A. N. Rubtsov, C. W. van Hasselt, M. A. C. Devillers, and Th. Rasing, *Phys. Rev. B* **54**, 1825 (1996); P. Godefroy, W. de Jong, C. W. van Hasselt, M. A. C. Devillers, and Th. Rasing, *Appl. Phys. Lett.* **68**, 1981 (1996).
- ³⁶J. Qi, W. Angerer, M. S. Yeganeh, A. G. Yodh, and W. M. Theis, *Phys. Rev. Lett.* **75**, 3174 (1995).
- ³⁷R. W. Kempf, P. T. Wilson, E. D. Mishina, O. A. Aktsipetrov, and M. C. Downer, *Appl. Phys. B: Lasers Opt.* **68**, 325 (1999).
- ³⁸P. T. Wilson, Y. Jiang, O. A. Aktsipetrov, E. D. Mishina, and M. C. Downer, *Opt. Lett.* **24**, 496 (1999).
- ³⁹O. A. Aktsipetrov, A. A. Fedyanin, J. I. Dadap, and M. C. Downer, *Laser Phys.* **6**, 1142 (1996).
- ⁴⁰C. Ohlhoff, G. Lüpke, C. Meyer, and H. Kurz, *Phys. Rev. B* **55**, 4596 (1997).
- ⁴¹C. W. van Hasselt, M. A. C. Devillers, Th. Rasing, and O. A. Aktsipetrov, *J. Opt. Soc. Am. B* **12**, 33 (1995).
- ⁴²C. W. van Hasselt, E. Mateman, M. A. C. Devillers, Th. Rasing, A. A. Fedyanin, E. D. Mishina, O. A. Aktsipetrov, and J. C. Jans, *Surf. Sci.* **331-333**, 1367 (1995).
- ⁴³O. A. Aktsipetrov, A. A. Fedyanin, E. D. Mishina, A. A. Nikulin, A. N. Rubtsov, C. W. van Hasselt, M. A. C. Devillers, and Th. Rasing, *Phys. Rev. Lett.* **78**, 46 (1997).
- ⁴⁴P. Thiansathaporn and R. Superfine, *Opt. Lett.* **20**, 545 (1995).
- ⁴⁵J. I. Dadap, J. Shan, A. S. Weling, J. A. Misewich, and T. F. Heinz, *Appl. Phys. B: Lasers Opt.* **68**, 333 (1999).
- ⁴⁶O. A. Aktsipetrov, I. M. Baranova, and Yu. A. Ilinskii, *Zh. Éksp. Teor. Fiz.* **91**, 287 (1986) [*Sov. Phys. JETP* **64**, 167 (1986)].
- ⁴⁷J. E. Sipe, D. J. Moss, and H. M. van Driel, *Phys. Rev. B* **35**, 1129 (1987).
- ⁴⁸P. Guyot-Sionnest, W. Chen, and Y. R. Shen, *Phys. Rev. B* **33**, 8254 (1986).
- ⁴⁹J. E. Sipe, *J. Opt. Soc. Am. B* **4**, 481 (1987).
- ⁵⁰C. G. B. Garrett and W. H. Brattain, *Phys. Rev.* **99**, 376 (1955).
- ⁵¹R. H. Kingston and S. F. Neustadter, *J. Appl. Phys.* **26**, 718 (1955).
- ⁵²S. M. Sze, *Physics of Semiconductor Devices* (Wiley, New York, 1981), Chap. 7, p. 362.
- ⁵³C. Kittel, *Introduction to Solid-State Physics* (Wiley, New York, 1956).
- ⁵⁴See, for a review, T. Ando, A. Fowler, and F. Stern, *Rev. Mod. Phys.* **54**, 437 (1982).
- ⁵⁵D. E. Aspnes and A. A. Studna, *Phys. Rev. B* **27**, 985 (1983).
- ⁵⁶E. H. Nicollian and J. R. Brews, *MOS (Metal Oxide Semiconductor) Physics and Technology* (Wiley, New York, 1982), Chap. 2, p. 26.
- ⁵⁷A. W. Stephens, A. G. Aberle, and M. A. Green, *J. Appl. Phys.* **76**, 363 (1994).
- ⁵⁸J. R. Power, J. D. O'Mahony, S. Chandola, and J. F. McGilp, *Phys. Rev. Lett.* **75**, 1138 (1995).
- ⁵⁹O. A. Aktsipetrov, A. A. Fedyanin, A. V. Melnikov, J. I. Dadap, X. F. Hu, M. H. Anderson, M. C. Downer, and J. K. Lowell, *Thin Solid Films* **294**, 231 (1997).
- ⁶⁰M. Cardona, *Modulation Spectroscopy*, edited by F. Seitz, D. Turnbull, and H. Ehrenreich, *Solid State Physics Suppl. 11* (Academic, New York, 1969).